Determination of the Magnetic Properties of Materials by a Method of Two Solenoids

Thomas Hartigan

Experiment performed 17/11/22

Abstract

This work aims to assess the reliability of determining magnetic material properties using a method of two solenoids. The magnetic flux density, B, induced within a sample, when subject to a magnetic field strength, H, was measured by integrating the electromotive force induced over a sufficiently long, straight solenoid surrounding the sample. The magnetic field strength H was applied by placing this arrangement within another, outer solenoid, within which H could be calculated when the current passing through this outer solenoid was known. This method was able to successfully determine the relative permeability of air as $\mu_{r,air} = 0.94 \pm 0.18$ and was also able to determine both the ferromagnetic and paramagnetic B vs H relationships for a sample of Cu/Ni Alloy below and above its Curie temperature respectively. Based on these observations it was determined that the method used yielded reliable data from which the magnetic material properties of a sample could be found. The applicability of this method was then demonstrated by evaluating the magnetic material properties, as well as the differential permeabilities for Mild Steel, Transformer Iron and a Cu/Ni Alloy. The maximum differential permeability, $\mu_{dif} = \frac{1}{\mu_0}\frac{dB}{dH}$ for Mild Steel, Transformer Iron and the Cu/Ni Alloy were found to be 134 ± 4, 280 ± 20 and 31.6 ± 0.7 respectively. [2997 Words].

1 Introduction

The material properties of ferromagnetic materials are important to understand due to their wide array of applications from transformers to data storage devices. In this work, the reliability of a non-destructive method to find magnetic material properties using two solenoids was evaluated by comparing the determined value for the relative permeability of air with the accepted value, and by successfully detecting the change in magnetic properties in a Cu/Ni Alloy above and below its Curie temperature. Values of the material properties; differential permeability, μ_{dif}, coercivity, H_c, remanence, B_r, saturation magnetisation, M_s, the applied field required to achieve the saturation magnetisation, H_{sat}, and the energy per unit volume required to flip the magnetisation direction within a material, u_{mag} were then found for Mild Steel, Transformer Iron and the Cu/Ni Alloy in its ferromagnetic phase. The relative permeability of the Cu/Ni alloy was also found in its paramagnetic phase.

Previous works [7] have demonstrated the applicability of similar processes in determining properties of material microstructures. The method proposed in this work could be used to rapidly gather datasets for different materials in the lab, for which this analysis could then be conducted.

An overview of the theory follows, then a description of the method and reporting of results in section 3. These results, assumptions, errors and applications are discussed in section 4 before reaching conclusions.

2 Theory

2.1 Ferromagnetic Hysteresis

A model of magnetism where the magnetic flux density, $\boldsymbol{B}$, is taken to be a linear combination of magnetic field strength, $\boldsymbol{H}$, and the magnetisation of material, $\boldsymbol{M}$, gives

$$\boldsymbol{B} = \mu_0(\boldsymbol{H} + \boldsymbol{M}). \tag{1}$$

Hence, in diamagnetic and paramagnetic materials where $\boldsymbol{M} = \chi_m \boldsymbol{H}$ and χ_m is a material constant, the above may be rewritten as

$$\boldsymbol{B} = \mu_0(1 + \chi_m)\boldsymbol{H} = \mu_r \mu_0 \boldsymbol{H}$$

where $\mu_r = (1 + \chi_m)$ is the relative permeability of the material. For ferromagnetic materials, $\boldsymbol{M}$ may be a function of H, often of the form shown in figure 1a. It is also helpful to define the differential permeability μ_{dif} of a material [3, p. 6], which is itself generally a function of $\boldsymbol{H}$ and gives the gradient of the B vs H graph.

$$\mu_{dif} = \frac{1}{\mu_0}\frac{dB}{dH}$$

A ferromagnetic material may be considered as many domains where the magnetic moments on each nucleus is aligned [6]. Each domain can be considered to have their own magnetisation vector, $\boldsymbol{M}_d$, where $\sum_d \boldsymbol{M}_d = \boldsymbol{M}$. Due to their underlying crystal structures, ferromagnetic materials tend to have preferred magnetisation directions, easy axes, along which each $\boldsymbol{M}_d$ will lie. When an applied field $\boldsymbol{H} < \boldsymbol{H}_{sat}$ is applied, the domain walls will move such that the domains all merge into one directed along the easy axis closest to the direction of the applied field. Application of field $\boldsymbol{H} \approx \boldsymbol{H}_{sat}$ will then cause this domain to rotate off the easy axis and in the direction of the applied field. This process is then reversed as the applied field decreases, eventually flipping the magnetisation direction; this gives rise to ferromagnetic hysteresis. For most ferromagnetic materials, there is a critical temperature, the Curie temperature T_c above which thermal agitation is sufficient to cause the magnetic moments on each nucleus to become randomly aligned, thus displaying paramagnetic properties [6].

The energy dissipated per unit volume during a hysteresis cycle, $u = \int H dB$ [4, eq. 36.22]. Hence, for any sample the energy required per unit volume to flip its magnetisation direction,

$$u_{mag} = \frac{1}{2}\int H dB.$$

It can be seen that this is directly proportional to the area of a hysteresis loop, such as in figure 1b. Where μ_0 is the permeability of free space, the relative permeability of a material may be defined as

$$\mu_r = \frac{B}{H\mu_0}, \tag{2}$$

however, it should be noted that this causes difficulties when evaluating μ_r at $H \approx 0$ during ferromagnetic hysteresis, so in these cases, differential permeability can be more informative.

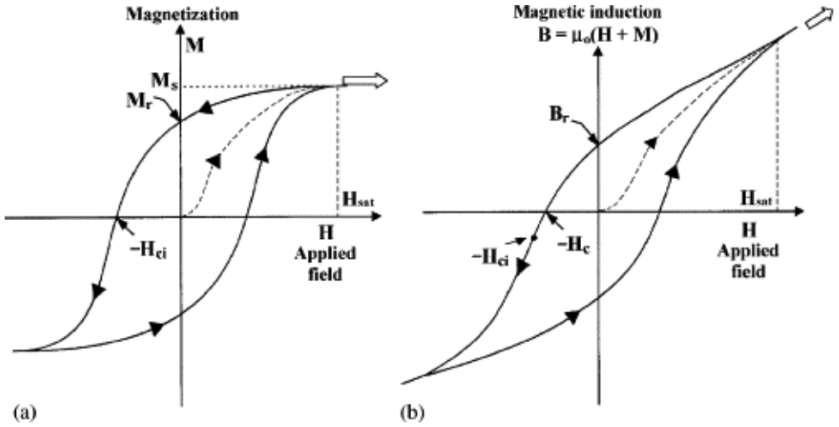

Figure 1: From [2] showing generic M vs H and B vs H curves seen in ferromagnetic hysteresis, each term is as defined in the Introduction and H_{ci} is the intrinsic coercivity.

2.2 Integrator Circuit

The circuit in figure 2 can be shown to integrate V_{in} when R_3 is a very large shunt resistor, such that it can be assumed very little current flows through R_3. The potential difference between the negative terminal of the op amp and ground, $V_- = 0$. Hence, where I_{in} is the current produced by the AC source, $V_{in} - V_- = I_{in}R_2$, $V_- - V_y = \frac{Q}{C}$ and $Q = \int I_{in}dt$, where $|Q|$ is the magnitude of charge stored on each plate of the capacitor. Combining the above, it is seen that

$$V_y = -\frac{1}{R_2 C}\int V_{in}dt. \tag{3}$$

2.3 Voltage Conversion

Assuming there are no free charges present, integrating Maxwell's fourth equation,

$$\boldsymbol{\nabla} \times \boldsymbol{H} = \boldsymbol{J}_{free} + \frac{\partial \boldsymbol{D}}{\partial t}$$

gives $\oint \mathbf{H} \cdot \mathbf{dl} = \int \mathbf{J} \cdot \mathbf{dA}$. Also assuming a solenoid can be modelled as if it is infinitely long (see Discussion), $|\mathbf{H}|$ outside the solenoid is always 0 [1, p. 236]. Hence, the magnetic field strength within a solenoid of length L with n_1 turns, subject to an AC current I, as in figure 3,

$$H = \frac{In_1}{L} = \frac{V_x n_1}{R_1 L}. \tag{4}$$

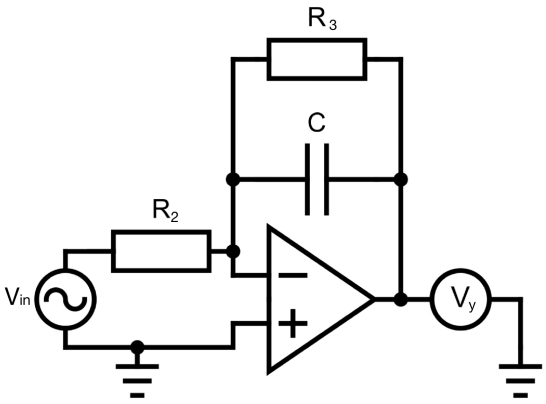

Figure 2: The integrator circuit used to find V_y

Faraday's law states that a change in magnetic flux will induce an electromotive force, emf,

$$\epsilon = \oint \boldsymbol{E} \cdot d\boldsymbol{l} = -\frac{d}{dt} \int_S \boldsymbol{B} \cdot d\boldsymbol{S}.$$

Hence, when another air-filled solenoid with cross-sectional area A_2 and n_2 turns is placed inside a solenoid with n_1 turns, and the inner solenoid is approximated as n_2 stacked loops, the induced emf between the top and bottom of the inner solenoid,

$$\epsilon_2 = -\frac{d}{dt} \int \boldsymbol{B_a} \cdot d\boldsymbol{S} = -n_2 A_2 \frac{dB_a}{dt} \tag{5}$$

where B_a is the magnetic flux density throughout the air region. This emf is then input to the integrator circuit described above, so using (3)

$$V_y = \frac{n_2 A_2}{R_2 C} \int \frac{dB_a}{dt} dt = \frac{n_2 A_2}{R_2 C} B_a$$

Hence,

$$B_a(V_y) = \frac{R_2 C V_y}{n_2 A_2} \tag{6}$$

If the inner solenoid itself also contains a sample of material with cross-sectional area A_m, then where $B_a(V_x)$ is a function of V_x,

$$\epsilon_2 = -\frac{d}{dt} \int \boldsymbol{B} \cdot d\boldsymbol{S} = -n_2 \frac{d}{dt} \left(B_m A_m + (A_2 - A_m) B_a(V_x) \right) \tag{7}$$

Using (3), (6) and (7), it can then be seen that

$$B_m = \frac{1}{A_m} \left(\frac{R_2 C V_y}{n_2} + (A_m - A_2) B_a(V_x) \right). \tag{8}$$

Hence, using (8), it is possible to find the magnetic flux density generated within a material when it is subjected to a specific magnetic field strength, and the magnetic flux density of air at that specific magnetic field strength is also known. Using (4) and (8), a B vs H hysteresis loop can be plotted.

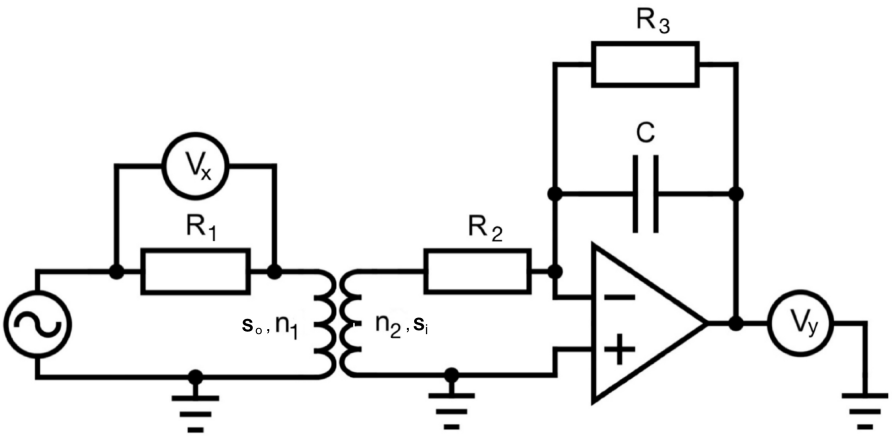

Figure 3: The circuit used to obtain each hysteresis loop

3 Method and Results

3.1 Air

According to (8), in order to determine the hysteresis loop and thus magnetic properties of arbitrary materials with $A_m < A_2$, where A_2 is the area of solenoid S_i described in Figure 4, the relationship for B vs H for air must be known. This relationship was found using the circuit in Figure 3 and the arrangement in Figure 4 where A_m is ignored, S_o and S_i are solenoids with n_1 and n_2 turns respectively, and S_o has length L.

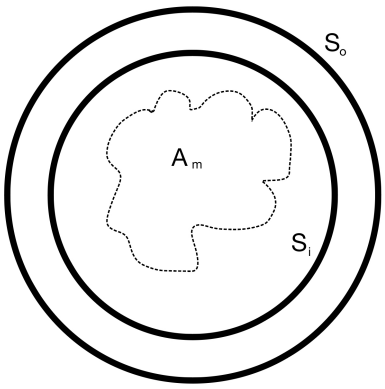

Figure 4: The geometry of solenoids and sample used. A_m represents the cross-sectional area of a material sample. S_o and S_i refer to the outer and inner solenoids respectively.

Properties of the components shown in Figure 3 were measured. The AC source produced 50Hz, 6V AC. $R_1 = 2.047 \pm 0.002\Omega$, $R_2 = 9.943 \pm 0.005k\Omega$, $R_3 = 976.0 \pm 0.1k\Omega$ and $C = 494.17 \pm 0.01nF$ were measured using an LCR metre. It was taken as given that $n_1 = 400$ and $n_2 = 500$. The geometry shown in Figure 4 was also recorded. The

length of S_o, $L = 4.487 \pm 0.005cm$ was found using the average of 5 vernier calliper measurements. $A_2 = 0.66 \pm 0.13cm^2$ was found by taking the mean of 5 measurements of the inner diameter and 5 measurements of the outer diameter of the material holding S_i. Here, the error in A_2 is taken as the standard deviation of the values measured without division by $\sqrt{n}$, for more details see the discussion. Two 10x scope probes were calibrated using square waves from a signal generator. One was used to measure V_x and the other V_y. The performance of the integrator part of the circuit shown in Figure 2 was tested around 50Hz using a signal generator and behaved as expected. The scopes measuring V_x and V_y were both set to AC mode, so only the variations in their signal were recorded. This method was chosen to decrease the size of each voltage bin and hence produce more precise values.

The setup shown in Figures 3 and 4 was used to collect values of V_x and V_y, which were then converted into $|\boldsymbol{H}|$ and $|\boldsymbol{B}|$ using (4) and (6). Linear regression was then applied to find a value of $\mu_{r,air} = 0.94 \pm 0.18$ where the errors in R_1, R_2, C, L and A_2 were added in quadrature. As there is expected to be very little energy dissipation to the air within S_i, the same loop area algorithm as is described below was applied to this dataset to obtain an estimate of its systematic error. The differential permeability was also calculated to demonstrate the limitations of the fitting model used, see figure 5 and the discussion.

(a)

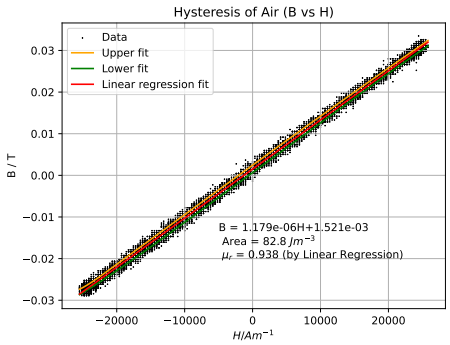

(b)

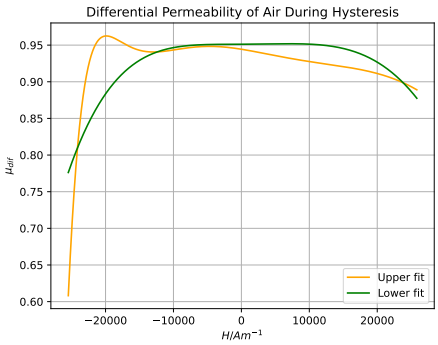

Figure 5: Plots showing (a) the measured B vs H relationship when S_i is contains only air, as well as (b) the differential permeability of air as a function of H. Error bars not plotted for neatness; underlying $\Delta V_x = 0.08V$ and $\Delta V_y = 0.016V$.

3.2 Materials

To find the properties of materials other than air, the geometries of the materials must also be known (8). Hence, A_m in Figure 4 was found for each material investigated (Table 1). Errors were obtained as usual for averages of repeat measurements.
For each material, the sample was placed within S_i and a respective dataset of V_x and V_y was taken. Using (8) and the B vs H relationship for air in Figure 5a, it was then

possible to find the magnetic flux density induced within each material using (8). These relationships are shown on the left side of Figure 6.

Material	$\boldsymbol{A_m/mm^2}$
Mild Steel	7.79 ± 0.03
Transformer Iron	3.16 ± 0.03
Cu/Ni Alloy	19.56 ± 0.05

Table 1: Cross-sectional areas of each material investigated.

The data was also computationally analysed, with each dataset of B vs H split into upper and lower datasets, where the upper dataset was taken as being all values of B within each small range of H, ΔH, which were greater than the average of all the values of B lying within ΔH, and vice versa for the lower dataset. Throughout each of the upper and lower datasets, an average value of B within each ΔH was then found, and these values were then fit using a linear combination of arbitrary hyperbolic tangent functions such as $\alpha \tanh(\beta H + \gamma) + \ldots$, determining $\alpha, \beta, \gamma, etc.$ The area enclosed by these fits was then found and is reported along with traces of each fit on the left side of Figure 6. The differential permeability was then also calculated by taking the gradient of each fit at each value of H, and these are plotted as functions of H on the right of figure 6.

Assuming that the true value of the B vs H area for air should be zero, this process produces a systematic offset of $82.8 Jm^{-3}$. This will be taken from the values displayed in figure 6 prior to any calculation. Each measured parameter, as well as the quantisation errors in V_x and V_y will contribute to the random error in the area. Using (8), a differential measurement of B between upper and lower sections of a hysteresis curve can be found as

$$B_{m,up} - B_{m,low} = \frac{R_2 C}{A_m n_2}(V_{y-avg,up} - V_{y-avg,low})$$

where $V_{y-avg,up}$ and $V_{y-avg,low}$ correspond to a specific V_x. Hence, approximating $V_{y-avg,up}$ for all V_x as $V_{y-max-avg}/2$, half of its peak amplitude, and $V_{y-avg,low}$ as $-V_{y-max-avg}/2$, the area enclosed can be crudely approximated as

$$A \approx H_{range} \frac{R_2 C}{A_m n_2} V_{y-max-avg}.$$

Assuming that $\Delta V_{y-max-avg} \approx \frac{\Delta V_y}{\sqrt{n_{Hb}}}$ where $n_{Hb} \approx 30$ is the average number of V_y values averaged in each upper or lower ΔH range, adding errors in quadrature gives

$$\Delta A \approx A \left(\left(\frac{\Delta R_2}{R_2} \right)^2 + \left(\frac{\Delta C}{C} \right)^2 + \left(\frac{\Delta A_m}{A_m} \right)^2 + \left(\frac{\Delta V_y}{n_{Hb} V_{y-max-avg}} \right)^2 \right)^{1/2},$$

where ΔV_y varies with the magnitude of the voltages being recorded, see Table 2.

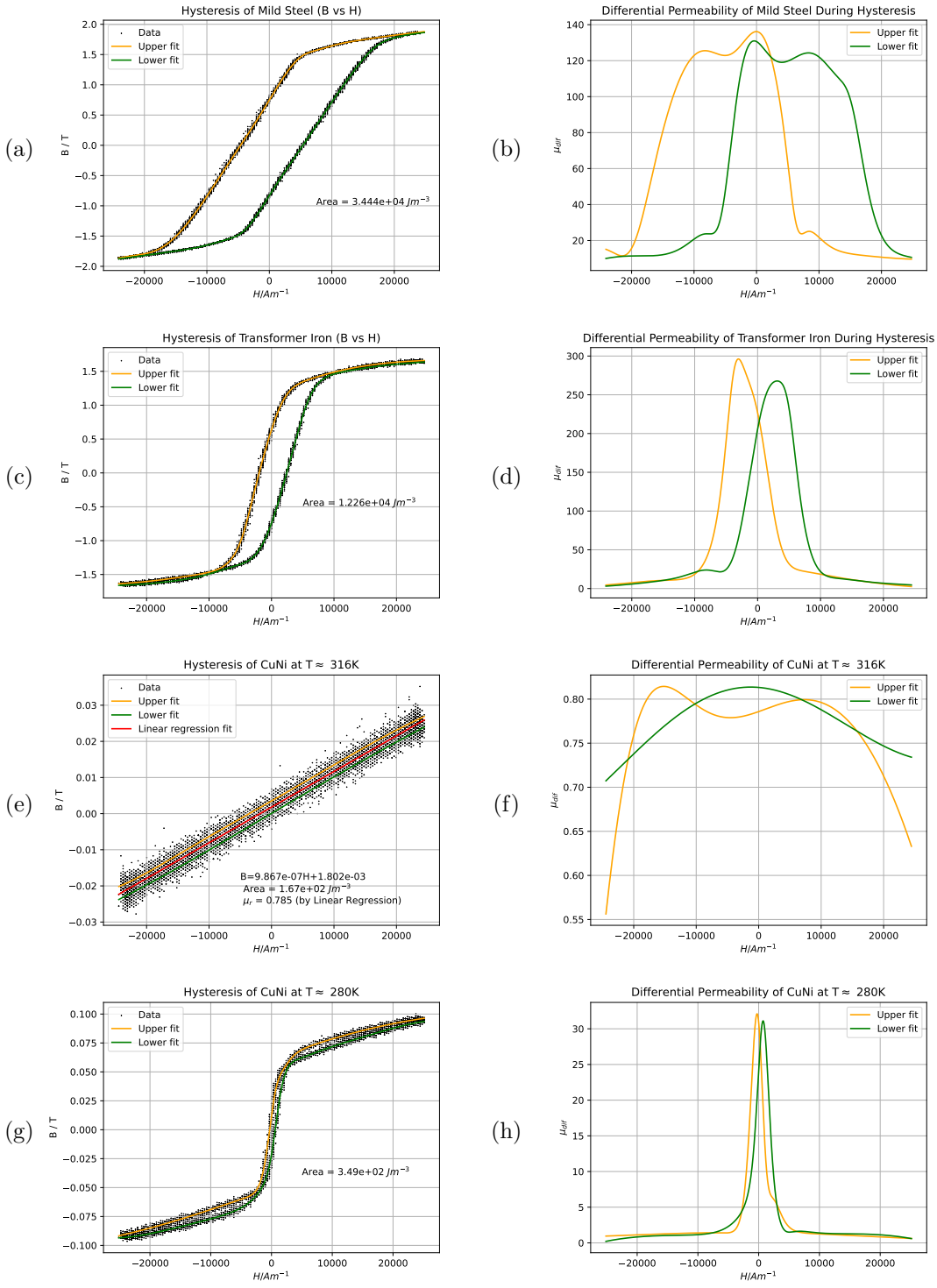

Figure 6: Plots showing each hysteresis curve measured (left) and the corresponding differential permeability of the material (right) as H varies. Error bars not plotted for neatness; underlying $\Delta V_x = 0.08V$ and ΔV_y can be seen in Table 2

Material	$\boldsymbol{\Delta V_y/V}$	$\boldsymbol{u_{mag}/Jm^{-3}}$
Mild Steel	0.016	17180 ± 70
Transformer Iron	0.008	6090 ± 60
Cu/Ni Alloy at 316K	0.0016	42.10 ± 0.11
Cu/Ni Alloy at 280K	0.004	133.1 ± 0.4

Table 2: Values of ΔV_y for each set of measurements and the energy required per unit volume to flip the magnetisation direction of the material, u_{mag}.

The graphs in figure 6 can also be used to estimate H_c, B_r, H_{sat} and M_s for each hysteric material, where B_{sat} was taken to be at the first point where the differential permeabilities of upper and lower fits are approximately equal (Transformer Iron), or $\mu_{dif} < 1.25$ for both curve fits (Cu/Ni). In theory, due to (1) H_c should lie where both fits give $\mu_{dif} \approx 1$ for a sufficiently large applied field. H_c was obtained by finding the values at which the upper and lower curve fits cross $B = 0$ and then averaging the absolutes of these values. A similar process was used to find B_r at x=0. M_s was found by measuring B_s, the average magnitude of each B at $\pm H_{sat}$ for both the upper and lower fits, and then using (1). The results can be seen in Table 3. Using a similar method of averaging as for H_c, the maximum values of μ_{dif} for Mild Steel, Transformer Iron and the Cu/Ni Alloy were found to be 134 ± 4, 280 ± 20 and 31.6 ± 0.7 respectively.

Material	$\boldsymbol{H_c/kAm^{-1}}$	$\boldsymbol{B_r/T}$	$\boldsymbol{H_{sat}/kAm^{-1}}$	$\boldsymbol{M_s/kAm^{-1}}$
Mild Steel	5.0 ± 0.5	0.79 ± 0.05	> 24.8	N/A
Transformer Iron	2.2 ± 0.3	0.69 ± 0.7	10.0 ± 0.9	1166 ± 16
Cu/Ni Alloy at 280K	0.5 ± 0.2	0.017 ± 0.007	16.2 ± 0.3	50 ± 3

Table 3: Values of the magnetic material properties obtained for each material.

At temperatures above around 213K, the Cu/Ni Alloy lost its ferromagnetic properties, and a linear B vs H relationship was seen as a result of passing the Curie temperature of the sample. Linear regression found a relationship of $B = \mu_0(0.785 \pm 0.001)H + 0.0018 \pm 2.11 \times 10^{-5}$ with $R^2 = 0.984$, as in Figure 6e. Assuming the non-zero B-intercept is negligible, and using (2), $\mu_r = 0.785 \pm 0.001$ for Cu/Ni Alloy above its Curie temperature, where only the linear regression error has been used (see discussion).

4 Discussion

4.1 Results

The value of $\mu_{r,air}$ agrees within error with the accepted value [5, p. 16], and the equipment was easily able to distinguish between the ferromagnetic and paramagnetic phases of the Cu/Ni Alloy sample, see Figures 6e and 6g. This confirms that the apparatus behaved as intended and the results obtained should therefore be accurate. The results in Figures 5, 6 and Tables 2 and 3 are also consistent with the applications of each material. E.g. u_{mag} is very small for transformer iron, despite still producing a very large M_s. Comparisons to accepted values cannot be given, as the exact sample compositions are unknown and general reference values for the material properties tested could not be readily found in the literature.

For the reported values of u_{mag}, fractional errors were seen to be small ($\approx 1/100$). However, particularly for the measurements taken directly from the hysteresis graphs in Table 3, the fractional errors are larger ($\approx 1/10$). This was in part due to slight asymmetries in the hysteresis curves measured, which are most likely due to an unidentified offset. Further work should be done to determine the cause of this offset. The uncertainty reported for the value of $\mu_{r,CuNi}$ was based solely on the linear regression error due to time limitations, so it is expected to substantially underestimate the true uncertainty.

4.2 Assumptions

In section 2.1, it is assumed that the outer solenoid may be treated as though it is infinitely long and hence $|\boldsymbol{H}| = 0$ everywhere outside the solenoid. This is not the case in practice, so edge effects will cause overestimates in the calculated values of H for any measured V_x. In this experiment, the exact diameter of S_o was not measured, so an exact diameter to length ratio cannot be given. An estimated ratio value using the maximum measured outer diameter of S_i gives $d_{outer}/L \approx 6$, so it is reasonable to assume these edge effects have only a small impact on results. Changes could be made to the experimental procedure to further minimise this effect.

The curve fitting models used throughout seemed to fit the data well. However, as seen in 5b and 6f, the fits appeared to curve quite significantly when modelling seemingly straight lines. This is somewhat unexpected, as a hyperbolic tangent function should be able to model a straight line where in $\alpha \tanh(\beta H + \gamma)$, $\beta \to 0$ and α gives the gradient. Given more time, different initial estimates of parameters, or different fitting functions could be used to investigate this further. Figures 6b, 6d and 6h each have small kinks around 20% up from their minimum values. This may be an inaccuracy caused by the curve fit as described above or could be the trace of another phenomenon. More firm conclusions about this could be reached by sufficiently reducing experimental noise.

4.3 Errors

Whilst undertaking the experiment, there was difficulty measuring the value of A_s precisely due to the construction of S_i. The coil was wrapped very densely, and was wrapped around a supporting material, which itself did not seem to have a uniform cross-sectional area. For this reason, measurements of the diameter were made at the inside and outside edges of the supporting material and then the propagated average and standard deviation of these were used as A_s. The material itself is also of some concern as its properties were never investigated. Hence, systematic errors may result from the assumption that all material inside the coil in (5) was air. The determined value of $\mu_r, air = 0.94 \pm 0.18$ does agree with the accepted value $\mu_r, air = 1.00000037$ [5, p.16], but does have a very large fractional error. This is almost entirely due to the large fractional error in A_s. Fortunately, this is mainly a small correction term in most of the experiment, but the values presented for the paramagnetic behaviour of Cu/Ni alloy are more easily influenced due to the smaller induced magnetic flux density within the material.

The data presented in figures 5 and 6 is limited in its precision by the quantisations of both V_x and V_y by the picoscope used. Reasonable measures were taken to mitigate this effect by using the picoscope AC mode to decrease the size of each voltage bin, but nevertheless, the quantisation is large enough that there are multiple cases where exactly the same values of V_x and V_y are recorded in the obtained dataset. This is not reflected in the figures, but if more time were available, plotting each datapoint with a normalised opacity reflecting the number of datapoints with that value would be instructive. All calculations were conducted using the full dataset, so this should not affect reported values.

Values of H_{sat} and thus M_s in Table 3 were determined by a somewhat arbitrary method, as the results did not fit the theory sufficiently well to test with $\mu_r = 1$ within the range of tested applied field strengths. In subsequent experiments it should be investigated whether the expected relation ($\mu_{dif} = 1$ for $H > H_{sat}$) occurs where $H > 25000 Am^{-1}$.

4.4 Applications

The use of this apparatus to detect changes in a Cu/Ni Alloy could potentially be helpful for precisely determining the Curie temperature of many materials, or determining the exact compositions of materials if the shape of the hysteresis graph is already determined for a particular temperature range. The ability to find u_{mag} also makes this non-destructive method useful for determining whether a material would be well suited to applications such as transformers.

5 Conclusion

The relative permeability of air found $\mu_{r,air} = 0.94 \pm 0.18$ agrees within error with the accepted value of 1.00000037 [5, p.16]. In the case of the Cu/Ni alloy distinct ferromagnetic and paramagnetic behaviours were seen below and above the Curie temperature ($\approx 313K$) respectively. On the bases of these results, it is believed that the method of two solenoids was successful in measuring the magnetic material properties of samples placed within S_i, and hence that the properties found for each material in Tables 2 and 3 are correct within their reported gaussian errors. The value of μ_r for the Cu/Ni Alloy above its curie temperature is believed to be a good estimate of the true value, but its error is believed to be much larger than is stated. The differential permeability relationships on the right of Figure 6 are believed to be good approximations of μ_{dif} as functions of H, however errors from the curve fitting method used limit their precision and should be used as nothing more than approximations.

References

[1] Griffiths, D. (2017). *Introduction to Electrodynamics* (4th ed.). Cambridge: Cambridge University Press. doi:10.1017/9781108333511.

[2] Sung, H.W.F.; Rudowicz, C. *Physics behind the magnetic hysteresis loop—A survey of misconceptions in magnetism literature.* J. Magn. Magn. Mater. 2003, 260, 250–260.

[3] Anderson, A.P. (2000). *Permeability and Hysteresis Measurement.* CRC Press LLC.

[4] Feynman, Richard P. (1963-1965). *The Feynman lectures on physics.* Reading, Mass. :Addison-Wesley Pub. Co.

[5] Cullity, B. D.; Graham, C. D. (2008) *Magnetic Materials* (2nd ed.). IEEE Press.

[6] Oliver, R. (2021). *NST IA Materials Sciences Materials for Devices.* University of Cambridge Department of Materials Science and Metallurgy.

[7] Karimian, N. et al.*Differential permeability behaviour of P9 and T22 power station Steels.* Journal of Magnetism and Magnetic Materials. 2014, 352, 81-90.